Iranian Journal of Materials Forming 12 (1) (2025) 18-27

Online ISSN: 2383-0042

IJMF

Iranian Journal of Materials Forming

Journal Homepage: http://ijmf.shirazu.ac.ir

Research Article

Deformation Behavior of Aluminum Alloy During Severe Plastic Deformation by Integrated Equal Channel Angular Pressing and Extrusion (ECAP-Extrusion)

A. Fardi Ilkhchy[1*] and A. Heidarzadeh[2,3]

[1] Department of Materials Science and Engineering, University of Bonab, Bonab, 5551395133, Iran
[2] Department of Materials Engineering, Azarbaijan Shahid Madani University, Tabriz, Iran
[3] Department of Materials and Metallurgy, Faculty of Mechanical and Energy Engineering, Shahid Beheshti University, Tehran, Iran

ARTICLE INFO

Article history:

Received 21 January 2025
Reviewed 8 February 2025
Revised 22 February 2025
Accepted 23 February 2025

Keywords:

Severe plastic deformation
Extrusion
Equal channel angular pressing
Finite element simulation

Please cite this article as:

Fardi Ilkhchy, A., & Heidarzadeh, A. (2025). Deformation behavior of aluminum alloy during severe plastic deformation by integrated equal channel angular pressing and extrusion (ECAP-extrusion). *Iranian Journal of Materials Forming*, *12*(1), 18-27. https://doi.org/10.22099/IJMF.2025.52239.1320

ABSTRACT

This study investigates the deformation behavior of commercially pure aluminum using finite element analysis, focusing on the combined equal channel angular pressing (ECAP) and extrusion process. The objective is to analyze the effects of die angle, extrusion ratio, and friction coefficient on the process and the resulting material properties. The findings indicate that a smaller die angle, higher extrusion ratio, and increased friction coefficient all contribute to a greater required process force. While friction between the sample and die wall disrupts uniform plastic strain distribution, increasing the die angle up to 110° and using an extrusion ratio of 6.25 enhance strain uniformity.

1. Introduction

Over the past few decades, researchers have increasingly utilized severe plastic deformation as a technique for processing ultrafine-grained and nanostructured materials [1]. Several methods have been developed to implement SPD in metallic materials. Among the most notable techniques are equal channel angular pressing (ECAP), accumulative roll bonding (ARB)[3], high-pressure torsion (HPT) [4], constrained groove pressing (CGP) [5], hydrostatic extrusion (HE)[6], cyclic extrusion compression (CEC) [7], rolling in a three high skew rolling mill [8], and extrusion with KOBO [9],

* Corresponding author
E-mail address: ali.fardi@ubonab.ac.ir (A. Fardi Ilkhchy)
https://doi.org/10.22099/IJMF.2025.52239.1320

multi-directional forging (MDF) [10], multi-channel spiral twist extrude (MCSTE) [11], Equal channel angular pressing–forward extrusion (ECAP–FE), as well as several newer methods that have emerged in recent years [12, 13]. Paydar et al. [12] successfully consolidated aluminum particles at 200 °C using ECAP–FE process, in which both ECAP and forward extrusion occur within a single die. Compared to conventional extrusion, FE-ECAP produced a finer grain structure and superior mechanical properties. In another study, they showed that applying extrusion back pressure during ECAP prevents surface cracking and enhances both the microstructure and mechanical properties by promoting shear deformation and increasing aluminum self-diffusion [13].

Segal et al. [14] initially introduced ECAP as a method for subjecting metallic materials to high plastic strain. Research in this field has demonstrated the effectiveness of ECAP in processing nanostructured materials. In this technique, a specimen of either circular or square in shape is passed within a specially designed die. The die consists of two intersecting channels, one vertical and one horizontal, both having the same cross-section. As the specimen is pushed into the channel by a ram, it undergoes significant shear strain at the intersection of the channels. The magnitude of strain at each deformation stage can be determined using the following equation [2]:

$$\varepsilon = \frac{1}{\sqrt{3}}\left[2\cot\left(\frac{\Phi+\Psi}{2}\right) + \Psi_{CSC}\left(\frac{\Phi+\Psi}{2}\right)\right] \qquad (1)$$

In this equation, Φ represents the die angle, while Ψ denotes the outer curvature angle at the intersection of the two channels. According to the relationship, the applied strain increases as both the channel angle and the outer curvature angle decrease. When the die angle is set at 90 degrees and the outer curvature angle of the intersecting channels is zero degrees, the sample experiences an equivalent strain of approximately one at each stage of deformation. In addition to these parameters, several other factors influence the magnitude of the applied strain and the uniformity of deformation. These include the friction coefficient between the sample and the die wall, the workability of the material, the strain rate sensitivity of the flow stress, the processing temperature, and the back pressure applied during the process. Ideally, a frictionless die-sample interface would result in perfectly uniform strain. However, in reality, friction, extrusion ratio, and die angle contribute to non-uniform strain and alter the microstructure [15]. Finite element methods (FEM) are widely employed to predict material behavior, offering valuable insights into deformation and enabling researchers to assess process parameters before conducting physical experiments [16]. Over the past two decades, FEM has been extensively used to analyze severe plastic deformation via equal channel angular pressing (ECAP) of aluminum alloys, focusing on parameters such as die angle, back pressure, and inner die angle [15, 17]. Xu et al. [18] found that die design and extrusion parameters significantly influence strain uniformity, with lower die angles and higher extrusion ratios promoting more even strain distribution. Djavanroodi & Ebrahimi [19] demonstrated that increased friction leads to non-uniform strain across the sample, particularly in post-extrusion zones. In another study, Abd EL AAL et al. [20] investigated the plastic deformation of pure aluminum under combined ECAP-direct extrusion using 3D FEM alongside experimental validation. Their findings indicated that strain distribution in the post-extrusion region varies due to material flow constraints, with the highest strain occurring near the die wall. Moreover, predicted microhardness values, based on effective plastic strain, closely matched experimental results. Microstructural analysis further confirmed the FEM predictions regarding strain and microhardness distributions.

While some studies have explored this topic, a comprehensive finite element analysis (FEA) of pure aluminum's deformation behavior during integrated ECAP-extrusion is lacking. This study aims to address this gap by investigating the deformation of commercially pure aluminum during the combined ECAP-extrusion process using FEM. Specifically, it examines the effects of the friction coefficient, die angle, and extrusion ratio on strain distribution. The findings of

this research could help optimize the ECAP-extrusion process, leading to enhanced material properties and improved performance.

2. Numerical Simulation of ECAP-Extrusion Process

In this research, a 3D finite element simulation was conducted using DEFORM 10.2 software to model the severe plastic deformation process via the combined equal channel angular pressing and extrusion method. Due to the plane symmetry of the forming method, only half of the die, sample, and ram were considered in the simulation, with the symmetry plane defined within the software. The sample was modeled as a cylindrical shape with a diameter of 10 mm and a height of 50 mm, meshed using 25,000 tetrahedral elements. A mesh independence test was performed by analyzing the plastic strain distribution and pressing force variations for different element counts. The optimal mesh size was determined based on a balance between computational accuracy and efficiency. The final mesh contained 25,000 tetrahedral elements, as further refinement did not yield significant changes in strain distribution or pressing force, confirming the dependability of the simulation results.

To ensure a comprehensive understanding of both individual and interaction effects of process parameters, a full-factorial method was chosen over alternative approaches like Taguchi or fractional factorial design. While these methods could have reduced the number of simulations needed, our aim was to conduct a comprehensive analysis without assumptions regarding parameter interactions. The die components were treated as rigid bodies in the simulation. Fig. 1 illustrates a three-dimensional view of the process and a two-dimensional sketch of the symmetry plane. The simulation investigated the influence of key process parameters on material deformation behavior. Three different die angles (90°, 100°, and 110°) were chosen for ECAP stage to examine their effect on strain distribution. (Fig. 1(b)). The extrusion ratio was analyzed by keeping the initial sample diameter at 10 mm, while varying the final diameters to 4 mm, 6 mm, and 8 mm to evaluate changes in material flow behavior. The effect of friction was explored by simulating the process under different friction coefficients (0, 0.1, 0.2, 0.3, and 0.4) to assess its impact on strain uniformity. The values of process variables (die angle, extrusion ratio, and friction coefficient) were chosen based on a combination of literature review, practical feasibility, and the requirement for detailed parametric analysis. The selected values ensured that the examined range covered realistic processing conditions while capturing significant changes in strain distribution and pressing force. A moderate step size was maintained between levels to prevent excessive computational costs, while ensuring accurate trend analysis. A wider gap between values could have overlooked important intermediate effects and potential non-linear relationships between process parameters and deformation behavior. By optimizing step sizes, we ensured that the outcomes provided clear insights into the influence of each parameter, while maintaining computational efficiency.

In all simulations, the ram movement speed was set at 10 mm/s, and the sample was modeled as a deformable body made of aluminum (AA1100), with its mechanical and thermal properties obtained from the DEFORM software library. It was assumed that 90% of the applied energy was converted into heat, while only 10% was used for plastic deformation of the sample. The accuracy of the numerical results was ensured through several key factors, including a mesh independence test, physical consistency, software reliability and boundary condition optimization.

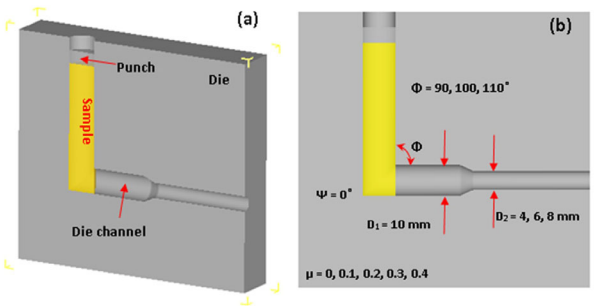

Fig. 1. (a) 3D representation of half of the ECAP-extrusion die, and (b) 2D view of the symmetry plane of the die indicating the different process parameters.

A mesh sensitivity analysis confirmed that further refinement beyond 25,000 tetrahedral elements did not significantly alter the results. The numerical trends of strain distribution and force variation aligned with fundamental principles of plastic deformation and previous experimental studies on ECAP-extrusion. Additionally, the use of DEFORM software, a well-established tool widely used for severe plastic deformation (SPD) simulations, provided further confidence in the results, as it employs validated material properties for AA1100 aluminum. The simulation parameters, including friction coefficient and ram speed, were carefully selected based on realistic process conditions to ensure practical relevance. While the current numerical approach provides reliable insights, future studies could incorporate additional experimental comparisons to further validate the simulation results.

3. Results and Discussion

3.1. Plastic strain distribution in the sample

Fig. 2 illustrates the impact of the friction coefficient on strain distribution within the sample, considering a die angle of 90 degrees and an extrusion output diameter of 6 mm. The results indicate that a completely uniform strain distribution is not achieved in any case, with different regions experiencing varying levels of plastic strain. Despite the symmetric geometry of the sample and die, ECAP-extrusion produces an asymmetric strain distribution due to three key factors: 1) Friction: The interaction between the die and sample introduces asymmetric shear forces, disrupting uniform material flow. 2) Sequential deformation: The combination of multi-stage ECAP shear and extrusion elongation leads to uneven strain accumulation. 3) Strain localization: Friction and material constraints cause higher strain near the die-wall interface.

The sample exhibits distinct regions with different strain values. The area before the intersection of the vertical and horizontal channels (marked in dark blue in Fig. 2) exhibits low strain values (Region I). Conversely, the region between the extrusion and equal channel angular pressing (Region II) experiences higher strain values. Within this region, plastic strain is non-uniform, with the bottom of the sample undergoing higher strain compared to the upper areas.

The presence of friction results in higher strain on the lower side of the sample, with the highest plastic strain occurring near the intersection of the vertical and horizontal channels (shown in red in Fig. 2). Increasing the friction coefficient intensifies the strain localization in the lower region while reducing the overall uniformity of the strain distribution. The dependence of strain in regions II and III on the friction coefficient arises primarily from the interaction between the sample and the die wall during deformation. As the friction coefficient increases, greater resistance develops at the sample-die interface, leading to higher shear stress and increased localized plastic deformation. This effect is most pronounced in region II, where material transitions from the ECAP zone to the extrusion phase. Lower friction, on the other hand, facilitates smoother material flow, resulting in a more uniform strain distribution. In region III (post-extrusion), strain distribution is influenced by material flow through the extrusion die. A higher friction coefficient restricts the movement of the outer layers more than the central region, increasing strain variations across the cross-section. As seen in Fig. 2, increasing friction shifts the strain concentration toward the lower side of the sample. Within region III, plastic strain is non-uniform with the highest strain observed in the upper and lower regions, while the central part experiences the least strain.

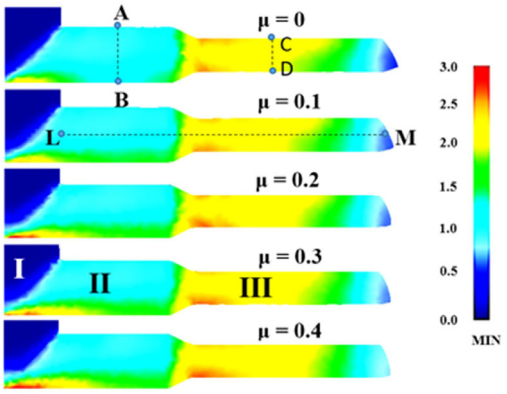

Fig. 2. Effect of the friction coefficient on strain distribution in the sample during the integrated ECAP-extrusion process.

Additionally, the magnitude of applied plastic strain gradually decreases towards the front of the sample. This indicates that in region III, the material undergoes both shear deformation from ECAP and elongation due to extrusion. The outer layers, in contact with the die walls, experience higher frictional resistance, leading to greater strain localization, whereas the central part flows more freely, creating a strain gradient. Furthermore, a higher extrusion ratio promotes increased elongation and a more uniform strain distribution. At lower extrusion ratios, strain localization is more pronounced, and the difference in strain between the outer and inner regions becomes more significant.

Fig. 3 illustrates the influence of die angle on strain distribution within the sample, considering a friction coefficient of 0.1 and an extrusion output diameter of 6 mm. The simulations show that the strain distribution remains non-uniform across all three regions of the sample for die angles of 90, 100, and 110 degrees. When the die angle is set to 90 degrees, the lower part of region II experiences the highest strain. However, as the die angle increases, the strain in the lower half of region II decreases, indicating that a larger die angle leads to a more uniform strain distribution in this region. Furthermore, increasing the die angle reduces the amount of strain applied to both the upper and lower areas of region III. This suggests that a higher die angle contributes to a more uniform strain distribution in region III as well. Despite these improvements, strain distribution across all three regions remains non-uniform for die angles of 90, 100, and 110 degrees.

Fig. 4 displays the effect of the extrusion ratio on strain distribution within the sample. A detailed analysis of the figure reveals several observations. The most uniform strain distribution in region II occurs when the extrusion output diameter is 4 mm, corresponding to an extrusion ratio of 6.25. In this case, the strain distribution across region II is relatively homogeneous. Moreover, for the extrusion ratio of 6.25, strain is distributed more homogeneously across region III. Under these conditions, strain is distributed more homogeneously across region III. Furthermore, at this extrusion ratio, region III also exhibits the most uniform strain distribution coinciding with the highest overall strain applied to the sample. This suggests that a higher extrusion ratio enhances strain uniformity in region III while increasing the total strain experienced by the material. Conversely, as the extrusion output diameter increases from 4 to 8 mm, reducing the extrusion ratio from 6.25 to 1.562, the strain distribution in regions II and III becomes progressively more uneven. Simultaneously, the overall strain applied in region III decreases. This reduction in uniformity and strain magnitude can be attributed to the lower extrusion ratio, which limits the material's elongation and affects its deformation behavior. At an extrusion ratio of 1.562, the central areas of region III exhibit the lowest strain, whereas the upper and lower surfaces of the sample experience the highest strain due to friction and additional shear stress.

In conclusion, the extrusion ratio plays a significant role in determining the strain distribution within the sample. A higher extrusion ratio tends to promote more uniform strain distribution, whereas a lower extrusion ratio results in greater strain variation and reduced overall strain, particularly in region III.

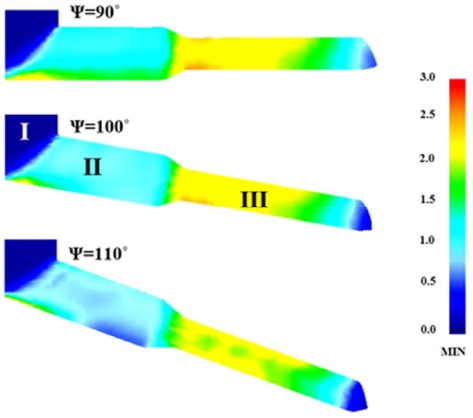

Fig. 3. Effect of ECAP die angle on strain distribution in sample during integrated ECAP-extrusion process.

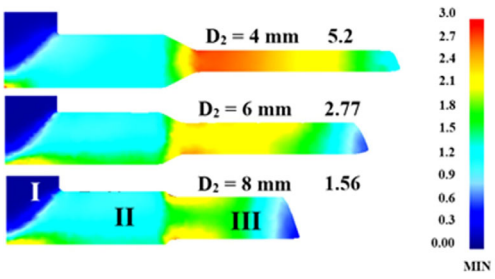

Fig. 4. Effect of extrusion ratio on strain distribution in sample during integrated ECAP-extrusion process.

3.2. Plastic strain variations across the sample

To further investigate the uniformity of plastic strain in the aluminum sample, the strain distribution was analyzed along the cross-section in the pre-extrusion region (line AB in Fig. 2).

Fig. 5(a) illustrates the impact of the friction coefficient on strain distribution. In all cases, the lower surface of the sample experiences higher deformation than the upper surface. As the friction coefficient increases, the strain on the lower surface intensifies, leading to a greater disparity in strain between the two surfaces. Fig. 5(b) presents the influence of the die angle on strain distribution across the sample's cross-section. At a die angle of 90 degrees, the lower surface undergoes more strain than the upper surface. However, as the die angle increases, the strain on the lower surface decreases. At 110 degrees, the deformation on the upper surface surpasses that of the lower surface, indicating that this angle results in the most uniform strain distribution. Fig. 5(c) demonstrates the influence of the extrusion ratio on strain distribution in the pre-extrusion area. The highest strain values occur in the upper regions of the sample. An extrusion ratio of 6.25 produces the smallest difference in strain between the upper and lower regions, suggesting that this ratio achieves the most uniform strain distribution. To quantitatively assess the uniformity of strain variations, the coefficient of variance of strain (CV_ε) is used. This coefficient is calculated using the following equation [21]:

$$CV_\varepsilon = \frac{Stdev(\varepsilon)}{Avg(\varepsilon)} \qquad (2)$$

Where *Stdev(ε)* represents the standard deviation of strain values at different points across the sample, and *Avg(ε)* is the average strain value.

Fig. 6 presents the calculated values of CV_ε for strain variations across the AB line (Fig. 2), indicating the effects of friction coefficient, ECAP die angle and extrusion ratio on the uniformity of plastic strain. Fig. 6(a) demonstrates the effect of the friction coefficient on CV_ε. Initially, CV_ε increases with friction but eventually stabilizes. This behavior can be attributed to two main factors: (1) Friction saturation: Beyond a certain threshold, increasing friction no longer significantly affects material flow or strain variation, and (2) Shear deformation dominates: Once shear localization is fully developed at the die-wall interface, additional friction does not significantly alter the strain distribution, leading to the stabilization of CV_ε. These results indicate that the friction between sample and die wall negatively impacts the uniformity of plastic strain variations in the pre-extrusion region.

Fig. 6(b) shows the relationship between CV_ε and the ECAP die angle. The results show a clear trend: CV_ε decreases as the die angle increases, meaning that a larger ECAP die angle improves strain uniformity in the pre-extrusion region. Fig. 6(c) illustrates the effect of the extrusion ratio on plastic strain uniformity.

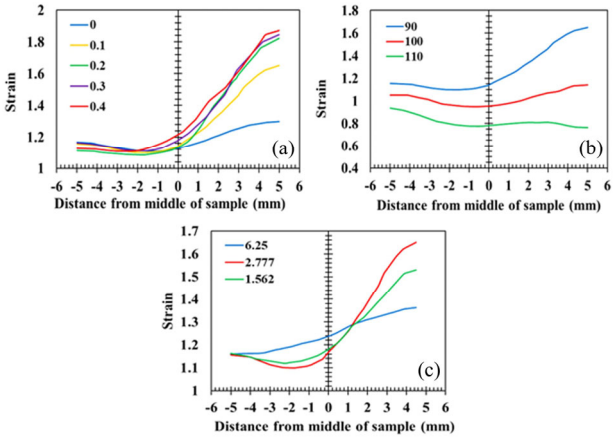

Fig. 5. (a) Effect of friction coefficient, (b) die angle, and (c) extrusion ratio on the variation of strain across the sample in the pre-extrusion area (AB line in Fig. 2).

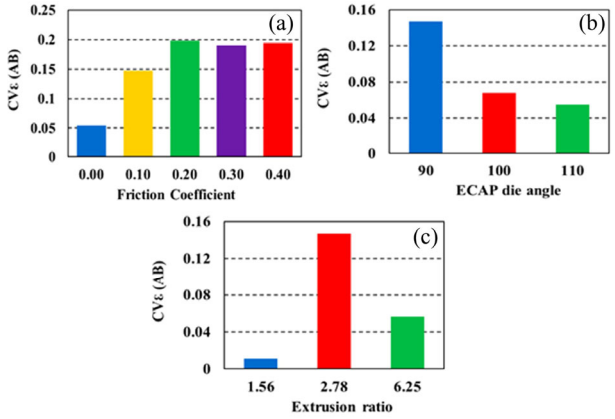

Fig. 6. (a) Effect of friction coefficient, (b) die angle, and (c) extrusion ratio on the coefficient of the variance of strain distribution (CV_ε) across the sample (AB line in Fig. 2).

Unlike the previous parameters, no straightforward correlation can be established between the extrusion ratio and the uniformity of strain distribution in the pre-extrusion region. The CV_ε value initially rises as the extrusion ratio increases from 1.562 to 2.777, then decreases when the extrusion ratio reaches 6.25. The lowest CV_ε and most uniform strain distribution are observed at an extrusion ratio of 1.562.

Fig. 7 illustrates the variations in plastic strain across the sample in the post-extrusion region (line CD in Fig. 2). Fig. 7(a) shows the impact of the friction coefficient on strain variations for an extrusion output diameter of 6 mm and a die angle of 90 degrees. In all cases, the upper part of the sample experiences greater strain than the lower regions. However, as the friction coefficient increases, the strain applied to the lower areas intensifies, leading to enhanced uniformity in the strain distribution along the CD line. Fig. 7(b) demonstrates the influence of the die angle on the variations in plastic strain across the cross-section of the sample along the CD line. Regardless of the die angle, the strain on the upper surface of the sample surpasses that of the lower surfaces. Additionally, as the die angle increases, the strain applied to the upper surface diminishes, while the deformation on the lower part of the sample increases. Fig. 7(c) illustrates the impact of the extrusion ratio on plastic strain variations across the sample. Increasing the extrusion ratio leads to higher strain in the lower regions of the sample, promoting a more uniform strain distribution through the CD line.

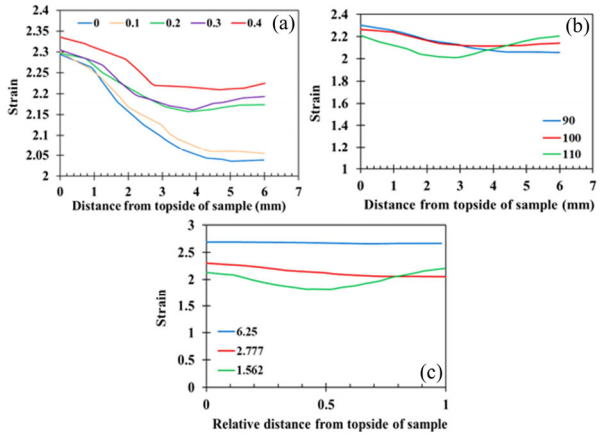

Fig. 7. (a) Effect of friction coefficient, (b) die angle, and (c) extrusion ratio on the strain distribution across the sample in the post-extrusion area (CD line in Fig. 2).

Fig. 8 shows the variations in CV_ε across the sample along the CD line (see Fig. 2) under different deformation parameters. Fig. 8(a) illustrates the effect of the friction coefficient, while Figs. 8(b) and 8(c) show the influence of the ECAP die angle and extrusion ratio, respectively. The results indicate that CV_ε decreases as the friction coefficient, ECAP die angle, and extrusion ratio increase. This suggests that higher values of these three parameters contribute to greater uniformity in plastic strain distribution across the sample in the post-extrusion region.

3.3. Plastic strain variations along the centerline of the sample

Fig. 9 shows the strain distribution along the longitudinal section and central axis of the sample (LM line in Fig. 2). Fig. 9(a) demonstrates the influence of the friction coefficient on strain variations along the central axis. Since the central axis is far from the surfaces, changes in the friction coefficient do not significantly affect the strain distribution. The overlapping curves indicate that strain distributions remain consistent across different friction values. The strain remains nearly constant at approximately 1.2 for the leftmost 20 mm of the sample, representing the initial stage. Moving rightward, the applied strain first exhibits a sharp increase, corresponding to the second stage of deformation (extrusion), followed by a gradual decrease. This reduction occurs because the rightmost regions of the sample experience less deformation across both stages.

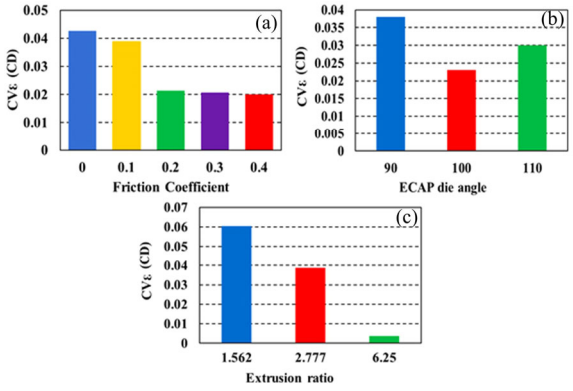

Fig. 8. (a) Effect of friction coefficient, (b) die angle, and (c) extrusion ratio on the coefficient of the variance of strain distribution (CV_ε) across the sample (CD line in Fig. 2).

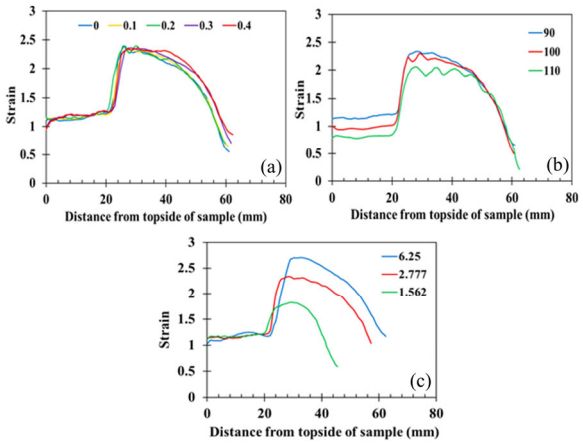

Fig. 9. (a) Effect of friction coefficient, (b) die angle, and (c) extrusion ratio on the strain distribution along the central axis of the sample (LM line in Fig. 2).

Fig. 9(b) presents the effect of the die angle on strain variations along the longitudinal axis. While the overall pattern of strain distribution remains unchanged, the magnitude of applied strain increases as the die angle decreases. Fig. 9(c) depicts the impact of the extrusion ratio on strain distribution. The applied strain in the pre-extrusion area remains relatively stable, while the strain in the post-extrusion area increases with a higher extrusion ratio. Among the three parameters analyzed, the extrusion ratio has the most significant impact on the applied strain.

Fig. 10 shows the effect of the friction coefficient, die angle, and extrusion ratio on the coefficient of variance of strain distribution (CV_ε) along the central axes of the sample (LM line in Fig. 2). As shown in Fig. 10(a), CV_ε decreases with an increasing friction coefficient, indicating a more uniform plastic strain distribution along the sample. Similarly, Fig. 10(b) shows that CV_ε decreases as the die angle increases, suggesting that a larger die angle results in a less uniform strain distribution along the centerline. Finally, Fig. 10(c) demonstrates that a higher extrusion ratio reduces the uniformity of strain distribution along the sample's centerline.

3.4. Pressing force

Fig. 11 illustrates the variation of pressing force over time under different conditions. At the initial stage of plastic deformation, the required pressing force is relatively low but gradually increases in two distinct phases: The first phase corresponds to the equal channel angular pressing (ECAP), while the second stage is associated with the extrusion process.

Fig. 11(a) shows the impact of the friction coefficient between the sample and the die wall, where increasing friction leads to a higher pressing force. Fig. 11(b) demonstrates that reducing the die angle results in a higher pressing force. Finally, Fig. 11(c) indicates that while the extrusion ratio has minimal effect on the force during the ECAP phase, it significantly increases the force required during the extrusion phase. Fig. 12 shows the effect of process parameters on the average force required for the entire process. The results demonstrate that an increase in the friction coefficient leads to a higher force requirement for both the ECAP and extrusion stage, ultimately raising the total pressing force (Fig. 12(a)).

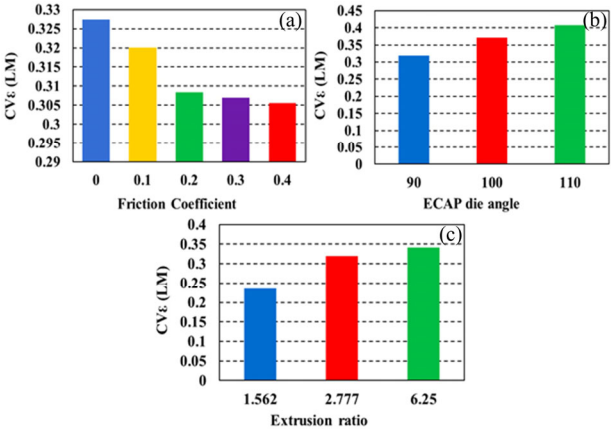

Fig. 10. (a) Effect of friction coefficient, (b) die angle, and (c) extrusion ratio on the coefficient of the variance of strain distribution (CV_ε) along the central line of the sample (LM line in Fig. 2).

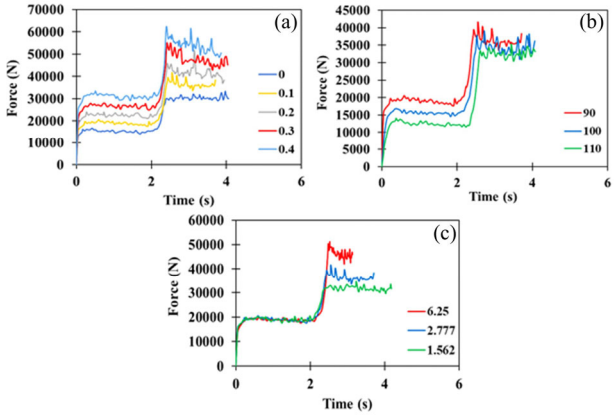

Fig. 11. (a) Effect of friction coefficient, (b) die angle, and (c) extrusion ratio on the variations of pressing force during integrated ECAP-extrusion process.

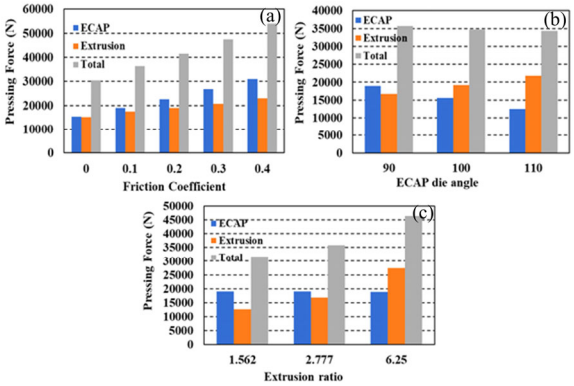

Fig. 12. (a) Effect of friction coefficient, (b) die angle, and (c) extrusion ratio on the average pressing force required for execution of the deformation process.

Due to the larger surface contact area and higher flow resistance during extrusion, the force required for this stage increases more significantly with friction compared to ECAP. As a result, the difference between the forces needed for these two stages grows as friction increases. Fig. 12(b) shows that decreasing the die angle reduces the force required for the ECAP stage but increases the force needed for extrusion. However, the overall effect on the total pressing force remains minimal. Fig. 12(c) reveals that increasing the extrusion ratio has little effect on the force required for the ECAP phase but significantly increases the force necessary for extrusion, leading to a higher total pressing force. At lower extrusion ratios, the forces required for ECAP and extrusion are more balanced. However, at an extrusion ratio of 6.25, the substantial reduction in sample cross-section during extrusion results in higher flow resistance, increased back pressure, and intensified strain hardening. Consequently, the pressing force required for extrusion becomes significantly greater than that for ECAP.

4. Conclusions

This study provides critical insights into optimizing the integrated ECAP-extrusion process by meticulously examining the influence of key parameters – friction, die angle, and extrusion ratio – on plastic strain distribution, uniformity, and required force. The findings indicate that minimizing friction is essential for achieving uniform strain distribution, as higher friction significantly increases strain inhomogeneity and raises the pressing force in both ECAP and extrusion stages. Furthermore, increasing the die angle reduces overall strain while improving strain uniformity, particularly in the post-extrusion region. The extrusion ratio also plays a crucial role in strain distribution. An extrusion ratio of 6.25 is found to provide the most uniform strain distribution in both pre- and post-extrusion regions, which is vital for maintaining consistent material properties. However, higher extrusion ratios also result in increased pressing force due to greater flow resistance and strain hardening effects. Furthermore, the analysis of the required force underscores the dominant role of friction in overall process efficiency. While the extrusion ratio primarily impacts the force required for extrusion, friction affects both ECAP and extrusion forces, making it a critical parameter for optimizing energy consumption. These findings offer valuable guidance for tailoring the ECAP-extrusion process to enhance material properties, improve strain uniformity and optimize energy efficiency.

Conflict of interest

The authors declare no conflict of interest.

Funding

This research received no specific grant from any funding agency in the public, commercial, or not-for-profit sectors.

5. References

[1] Toth, L. S., & Gu, C. (2014). Ultrafine-grain metals by severe plastic deformation. *Materials Characterization, 92*, 1-14. https://doi.org/10.1016/j.matchar.2014.02.003

[2] Furukawa, M., Horita, Z., Nemoto, M., & Langdon, T. G. (2001). Review: Processing of metals by equal-channel angular pressing. *Journal of Materials Science, 36*, 2835-2843. https://doi.org/10.1023/A:1017932417043

[3] Ghalehbandi, S. M., Malaki, M., & Gupta, M. (2019). Accumulative roll bonding—a review. *Applied Sciences, 9*(17), 3627. https://doi.org/10.3390/app9173627

[4] Reis, L. M., Hohenwarter, A., Kawasaki, M., & Figueiredo, R. B. (2024). Evaluating high-pressure torsion scale-up. *Advanced Engineering Materials, 26*(19), 2400175. https://doi.org/10.1002/adem.202400175

[5] Kumar, S. (2023). Developing methods of constrained groove pressing technique: A review. *Proceedings of the Institution of Mechanical Engineers, Part L: Journal of Materials: Design and Applications, 237*(6), 1319-1346. https://doi.org/10.1177/14644207221143358

[6] Garbacz, H., Topolski, K., & Motyka, M. (2019). Hydrostatic extrusion. In *Nanocrystalline Titanium* (pp. 37-53). Elsevier.

[7] Ebrahimi, M., Wang, Q., & Attarilar, S. (2023). A comprehensive review of magnesium-based alloys and composites processed by cyclic extrusion compression and the related techniques. *Progress in Materials Science, 131*, 101016. https://doi.org/10.1016/j.pmatsci.2022.101016

[8] Pater, Z., Tomczak, J., & Bulzak, T. (2020). Problems of forming stepped axles and shafts in a 3-roller skew rolling mill. *Journal of Materials Research and Technology, 9*(5), 10434-10446. https://doi.org/10.1016/j.jmrt.2020.07.062

[9] Dutkiewicz, J., Kalita, D., Maziarz, W., Tański, T., Borek, W., Ostachowski, P., & Faryna, M. (2020). Effect of KOBO extrusion and following cyclic forging on grain refinement of Mg–9Li–2Al–0.5Sc Alloy. *Metals and Materials International, 26*(7), 1004-1014. https://doi.org/10.1007/s12540-019-00350-y

[10] Manjunath, G. A., Shivakumar, S., Fernandez, R., Nikhil, R., & Sharath, P. C. (2021). A review on effect of multi-directional forging/multi-axial forging on mechanical and microstructural properties of aluminum alloy. *Materials Today: Proceedings, 47*, 2565-2569. https://doi.org/10.1016/j.matpr.2021.05.056

[11] Fouad, D. M., Moataz, A., El-Garaihy, W. H., & Salem, H. G. (2019). Numerical and experimental analysis of multi-channel spiral twist extrusion processing of AA5083. *Materials Science and Engineering: A, 764,* 138216. https://doi.org/10.1016/j.msea.2019.138216

[12] Paydar, M. H., Reihanian, M., Bagherpour, E., Sharifzadeh, M., Zarinejad, M., & Dean, T. A. (2009). Equal channel angular pressing-forward extrusion (ECAP-FE) consolidation of Al particles. *Materials and Design, 30*(3), 429-432. https://doi.org/10.1016/j.matdes.2008.06.012

[13] Paydar, M. H., Reihanian, M., Bagherpour, E., Sharifzadeh, M., Zarinejad, M., & Dean, T. A. (2008). Consolidation of Al particles through forward extrusion-equal channel angular pressing (FE-ECAP). *Materials Letters, 62*(17–18), 3266-3268. https://doi.org/10.1016/j.matlet.2008.02.038

[14] Segal, V. M., Reznikov, V. I., Dobryshevshiy, A. E., & Kopylov, V. I. (1981). Plastic working of metals by simple shear. *Russian Metallurgy (Metally), 1,* 99-105.

[15] Hans Raj, K., Sharma, R. S., Sahai, A., & Gupta, N. K. (2013). Different die designs for processing of al alloy using equal channel angular pressing: A FEM study. *Proceedings of the Indian National Science Academy, 79*(4), 829-836. https://doi.org/10.16943/ptinsa/2013/v79i4/48011

[16] Lyu, Y. (2022). *Finite element method: Element solutions*, Springer Singapore. https://doi.org/10.1007/978-981-19-3363-9

[17] Yoon, S. C., & Kim, H. S. (2008). Finite element analysis of the effect of the inner corner angle in equal channel angular pressing. *Materials Science and Engineering: A, 490*(1–2), 438-444. https://doi.org/10.1016/j.msea.2008.01.066

[18] Xu, S., Zhao, G., Ma, X., & Ren, G. (2007). Finite element analysis and optimization of equal channel angular pressing for producing ultra-fine grained materials. *Journal of Materials Processing Technology, 184*(1–3), 209-216. https://doi.org/10.1016/j.jmatprotec.2006.11.025

[19] Djavanroodi, F., & Ebrahimi, M. (2010). Effect of die channel angle, friction and back pressure in the equal channel angular pressing using 3D finite element simulation. *Materials Science and Engineering: A, 527*(4–5), 1230-1235. https://doi.org/10.1016/j.msea.2009.09.052

[20] Abd El Aal, M. I. (2017). 3D FEM simulations and experimental validation of plastic deformation of pure aluminum deformed by ECAP and combination of ECAP and direct extrusion. *Transactions of Nonferrous Metals Society of China, 27*(6), 1338-1352. https://doi.org/10.1016/S1003-6326(17)60155-9

[21] Basavaraj, V. P., Chakkingal, U., & Kumar, T. P. (2009). Study of channel angle influence on material flow and strain inhomogeneity in equal channel angular pressing using 3D finite element simulation. *Journal of Materials Processing Technology, 209*(1), 89-95. https://doi.org/10.1016/j.jmatprotec.2008.01.031